Virtual Resistor Active Damping with Selective Harmonics Control of LCL-Filtered VSCs

Wu, Yang; Soeiro, Thiago Batista; Shekhar, Aditya; Xu, Junzhong; Bauer, Pavol

DOI
10.1109/PEMC48073.2021.9432569

Publication date
2021

Document Version
Accepted author manuscript

Published in
Proceedings - 2021 IEEE 19th International Power Electronics and Motion Control Conference, PEMC 2021

Citation (APA)
Wu, Y., Soeiro, T. B., Shekhar, A., Xu, J., & Bauer, P. (2021). Virtual Resistor Active Damping with Selective Harmonics Control of LCL-Filtered VSCs. In *Proceedings - 2021 IEEE 19th International Power Electronics and Motion Control Conference, PEMC 2021* (pp. 207-214). Article 9432569 (Proceedings - 2021 IEEE 19th International Power Electronics and Motion Control Conference, PEMC 2021). IEEE. https://doi.org/10.1109/PEMC48073.2021.9432569

Virtual Resistor Active Damping with Selective Harmonics Control of LCL-Filtered VSCs

Yang Wu[1], Thiago Batista Soeiro[1], Aditya Shekhar[1], Junzhong Xu[2] and Pavol Bauer[1]
1: *DCE&S group*, *Delft University of Technology*, Delft, The Netherlands
2: *Department of Electrical Engineering*, *Shanghai Jiao Tong University*, Shanghai, China
Y.Wu-6@tudelft.nl, T.BatistaSoeiro@tudelft.nl, A.Shekhar@tudelft.nl, Junzhongxu@situ.edu.cn P.Bauer@tudelft.nl

***Abstract*—LCL filter is widely adopted for strict standard compliance of grid-tied voltage source converters (VSCs). The third order low-pass filtering provides great attenuation for the high frequency harmonics generated by the power electronics guaranteeing low output currents noise injection into the grid. A major concern of the implementation of the LCL-filter is to safeguard the system stability by providing effective damping of the filter resonances. Active damping methods are preferred because it does not result in substantial power losses as it would result by the utilization of passive damping circuits. Capacitor-current active damping (CCAD) technique can be effective while realizing only a proportional feedback. However, the suitable feedback gain for maintaining stability remains to be identified. Another control issue related to the grid-tied VSC is the harmonics compensation of the currents due to the grid voltage distortion. Therefore, this paper proposes an improved resonator with phase compensation to suppress the harmonics distortion while maintaining stability with properly design capacitor current feedback. The capacitor feedback gain for stability is analytically derived in this paper. The proposed control scheme is verified by both simulation and experimental results.**

***Index Terms*—Capacitor-current feedback Active damping (CCAD), Harmonics resonator, LCL filter, VSC**

I. Introduction

Pulse-Width Modulated (PWM) voltage source converters (VSCs) are the main building blocks for interfacing distributed generation (DG) units, power flow control and emerging smart loads with hybrid ac-dc distribution grids [1]–[4]. Continuous PWM strategy such as Sinusoidal PWM (S-PWM) is widely used for the modulation of VSCs due to the simplicity and better harmonics performance, instead of discontinuous PWM strategies [5], [6]. LCL filter is preferably adopted in VSCs for attenuating high frequency harmonics in the output waveforms. However, special attention must be paid to the LCL filter resonance which usually needs to be damped to safeguard the system stability. In renewable generation applications the grid-connected VSCs are generally controlled in Current-Control Mode (CCM). The choice of the converter or grid-side current control is influenced by the resonance of LCL filter based on the ratio between the resonance frequency f_{r} and the PWM sampling frequency f_{s} [7]. Recently, studies on the single-loop control revealed that the grid-side current control can be more stable if the the resonance frequency f_r lies between $\frac{1}{6}$ f_{s} (critical frequency) and $\frac{1}{2}$ f_{s} (Nyquist frequency) if the symmetric sampling and single-update PWM pattern is adopted [8]. For the double-update case, the critical frequency shifts to $\frac{1}{4}$ f_{s} [9]. Correspondingly, stability with converter-side current control can be ensured without any additional means if the f_{r} is found below the critical frequency.

This research has been funded within the Power2Power project, which is a European co-funded innovation project on Semiconductor Industry. The project receives grants from the European H2020 research and innovation program, ECSEL Joint Undertaking, and National Funding Authorities from eight involved countries under grant agreement No. 826417. The participating countries are Austria, Finland, Germany including the Free States of Saxony and Thuringia, Hungary, the Netherlands, Slovakia, Spain and Switzerland.

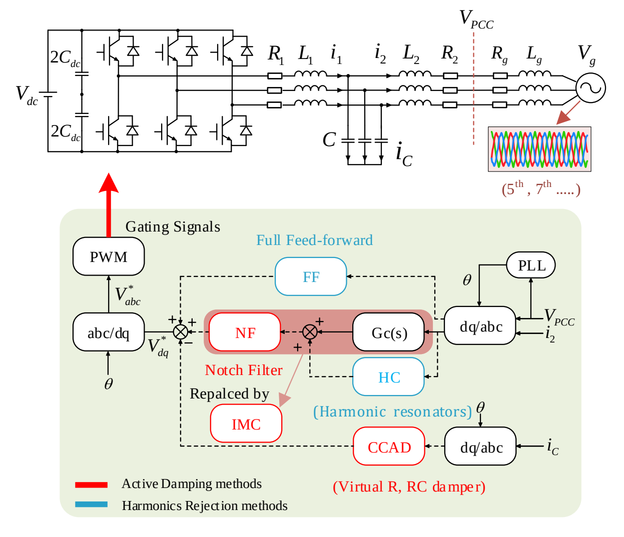

Fig. 1. Three-phase grid-tied voltage source converter with a LCL filter.

Achieving stable control is possible while operating in the previously described unstable control region defined by the chosen LCL filter and sampling frequency. However, a filter resonance damping measures becomes necessary for guaranteeing enough stability margin for the system. Passive damping solutions, i.e., parallel or series connection of resistor with the capacitor and/or inductor offers satisfactory performance but has consequence on the overall size and system efficiency [10]. On the other hand, the active damping schemes can improve the stability while not influencing the efficiency [7]–[9]. These methods can be classified into two main categories [8], [11], [12]: 1) multi-loop control methods; and 2) filter-cascaded methods.

The filter-based active damping methods, shown in Fig.1, are mainly realized by cascading the filter in the current controller loop. The notch filter (NF) method typically employs a second order digital filter which creates an anti-resonance at the pre-set LCL filter resonance frequency to improve the system attenuation around this frequency [11], [13]. Other filter-based methods, i.e, IMC (Internal Model Control) is derived based on the model of the control plant and are studied in [14]. However, both the NF and IMC model are sensitive to system parametric variations, e.g, the change of the LCL filter component values with the current bias and/or the intrinsic unknown grid impedance (represented by L_g and R_g in Fig.1). The adaptive or self-commissioned filter methods are proposed in [15] to improve the robustness against the circuit parametric uncertainties and dynamic variations, however, at the cost of control complexity. On the other hand, the multi-loop active damping method uses the available state signals in the circuit through feedback control to form an equivalent virtual resistor in series or parallel with the LCL filter elements, e.g., the filter capacitor and inductors. While both capacitor voltage and current feedback based control have been reported, cost of the voltage sensor can be lower compared to the high-bandwidth current ones. On the other hand, capacitor voltage active damping (CVAD) [16] requires the implementation of the differentiators in the feedback loop, which is difficult to implement in practice. By contrast, capacitor current active damping (CCAD), shown in Fig.1, only requires a proportional feedback [17]. If the influence of the digital control delay is considered, the proportional feedback of the capacitor current may result in a negative virtual resistor in some cases [12], leading to an undesired non-minimum phase system. However, this negative virtual resistor can be avoided if the resonance frequency is smaller than $\frac{1}{6}$ f_s with maximum possible delay.

Another control issue in a grid-connected VSC system is the control of the current harmonics due to the distorted grid voltage. Full feed-forward (FF) scheme of the grid voltage is reported to be able to effectively compensate the harmonics by fully canceling out the influence of the grid voltage [18]. However, full FF scheme needs to implement the first and second-order differentiators which is hard to precisely discretize in the digitally controlled system. In contrast, harmonic resonant controller is widely adopted to realize the selective harmonics compensation, which enlarges the loop gain at the tuned frequency. From the control point of view, the harmonics current can be suppressed due to the infinitely large grid impedance at the harmonics frequencies [2], [19], [20]. However, a resonator controller requires phase compensation [20], [21] to ensure enough phase margin due to the system delay. In this paper, an improved harmonics resonator with phase compensation along with a design guideline for capacitor current active damping is presented. The main contributions are 1) The analytical derivation of suitable capacitor current feedback gain ensuring system stability 2) The derivation of an improved resonator controller with phase compensation.

Section II presents the system description and basic control scheme. The analysis of capacitor current active damping and harmonics control are introduced in Section III and IV respectively. Simulations and experimental results are carried out in Section V. Conclusion and future work are presented in Section VI.

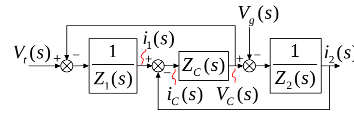

Fig. 2. Block diagram of the control plant of LCL-filtered VSC.

II. System Modeling and Control

A. Circuit Modeling

The VSC connected to the grid with a LCL filter is depicted in Fig. 1. The described grid is assumed to be a stiff grid which contains low-order harmonics such as 5_{th}, 7_{th}, 11_{th} and 13_{th}. Therefore, the grid interface components R_{g} and L_{g} are neglected in this paper and hence, $V_{\text{PCC}} = V_{\text{g}}$. The filter resistors R_1 and R_2 represent the internal resistance of the converter-side inductor L_1 and grid-side inductor L_2, respectively. Additionally, the equivalent resistance due to the conduction losses of the VSC is incorporated into R_1. Fig.2 shows the average switched model of the control plant of a VSC with LCL filter, where $V_{\text{t}}(s)$ is the VSC terminal voltage. The $Z_1(s)$, $Z_2 s$ and $Z_{\text{C}}(s)$ are the impedance of L_1, L_2 and C and given as:

$$Z_1(s) = sL_1 + R_1 \tag{1}$$

$$Z_2(s) = sL_2 + R_2 \tag{2}$$

$$Z_C(s) = \frac{1}{sC} \tag{3}$$

The transfer function relating the grid-side output current i_2 and the converter terminal voltage V_t is:

$$G_{\text{i}_2}(s) = \frac{i_2(s)}{V_{\text{t}}(s)} = \frac{1}{\alpha s^3 + \beta s^2 + \gamma s + \delta} \tag{4}$$

where, constants are given by $\alpha = L_1 L_2 C$, $\beta = R_2 L_1 C + R_1 L_2 C$, $\gamma = R_1 R_2 C + L_1 + L_2$ and $\delta = R_1 + R_2$. Considering that R_1 and R_2 are negligible, (4) can be simplified and given by (5).

$$G_{\text{i}_2}(s) = \frac{1}{L_1 L_2 C s}\left(\frac{1}{s^2 + \omega_{\text{r}}^2}\right) \tag{5}$$

where, the resonance frequency (ω_{r}) of the LCL filter is given by (6).

$$\omega_r = \sqrt{\frac{L_1 + L_2}{L_1 L_2 C}} \tag{6}$$

B. Basic Control of the VSC

The block diagram of the grid-side current control of VSC without any active damping and harmonics compensation is shown in Fig. 3.

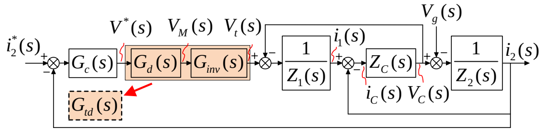

Fig. 3. Block diagram of the basic VSC grid current control scheme without active damping and harmonic suppression.

The compensator $G_c(s)$ used for current control is typically a PR (proportional-resonant) controller in stationary ($\alpha\beta$) frame or a PI controller in rotating (dq) frame [2], [19].

$$\begin{aligned} G_{c(\alpha\beta)}(s) &= k_p + \frac{k_r s}{s^2+\omega_1^2} \\ G_{c(dq)}(s) &= k_p + \frac{k_i}{s} \end{aligned} \tag{7}$$

The control and computation delay in the digitally controlled system is noted as $G_c(s)$. The mechanism of the computation delay depends on the sampling and update of the implemented PWM [17]. If the symmetric sampled PWM with single update (sampling happens at the upper peak of the triangular wave) is adopted, the computation delay is given by $G_d(s) = e^{\text{-sT}_s}$. f_s and f_{sw} are the sampling and switching frequency respectively such that $T_s = \frac{1}{f_s}$ and $T_{sw} = \frac{1}{f_{sw}}$. $G_{inv}(s)$ is the transfer function representing the PWM process, which is given by (8).

$$G_{inv}(s) = \frac{K_{pwm} G_h(s)}{T_s} \tag{8}$$

where, the PWM gain K_{pwm} is the ratio of the dc voltage V_{in} and amplitude of the triangular carrier wave V_{tri} and taken as 1 to simplify the analysis.

The Zero-Order Hold (ZOH) characteristics of the PWM process is modeled as an equivalent transfer function $G_h(s)$ as approximated by (9) using frequency domain analysis.

$$G_h(s) = \frac{1-e^{\text{-sT}_s}}{s} \approx T_s e^{\text{-}\frac{1}{2}\text{sT}_s} \tag{9}$$

Combining (8) and (9), the total delay G_{td} can be expressed as (10).

$$G_{td}(s) \approx e^{\text{-}\frac{3}{2}\text{sT}_s} \tag{10}$$

III. Capacitor Current Feedback Active Damping

A. Virtual Resistor

The allowable gain while ensuring stable operation of a VSC is limited when no active damping is used, as shown in Fig. 4 where the maximum controller gain is limited to $K_{ad} = 0.5$. Table. I lists the used parametric specifications.

TABLE I
System Parameters

L_1 , L_2	R_1 , R_2	C	V_{DC}	k_p	k_r	k_{rh}	ω_c
1.5 mH	0.2 Ω	20 μF	700 V	5	2500	1000	2

As a consequence, the small bandwidth of the closed-loop system leads to undesired slow system response. Consider the equivalent circuit of the LCL filter with capacitor current i_c shown in Fig. 5. The feedback of i_c is equivalent to adding an impedance ($Z_{ad} = R_{ad} + jX_{ad}$) in parallel with the filter capacitor [12].

In CCAD, the current control loop is modified using feedback of i_c via gain $K_{ad}(s)$ as shown in Fig. 6. The relation between Z_{ad} and $K_{ad}(s)$ is described by (11).

$$Z_{ad}(s) = \frac{L_1}{K_{ad}(s) G_{td}(s) C} \tag{11}$$

Without consideration of the delay $G_{td}(s)$, the equivalent impedance behaves like a virtual resistor if the proportional feedback gain K_{ad} is used [12], which is expressed by (12):

$$R_{ad} = \frac{L_1}{K_{ad} C} \tag{12}$$

However, the proportional feedback results in the virtual impedance if the system delay is included. By substituting (10) into (12), the impedance can be derived as (13):

$$Z_{ad}(s) = \frac{L_1}{K_{ad} C} e^{\text{-sT}_s} = R_{ad} e^{\text{-sT}_s} \tag{13}$$

Substituting $s = j\omega$ yields (14).

$$Z_{ad}(j\omega) = R_{ad}\ [cos(\frac{3}{2}\omega T_s) + jsin(\frac{3}{2}\omega T_s)] \tag{14}$$

As noted in (14), the delay influences both the resistive and inductive (or capacitive) parts. The imaginary term may alter the LCL filter resonance frequency and influence the precision of the control [16]. Meanwhile, it can be proven that the resistive part becomes negative when the frequency f ($\omega/2\pi$) is above $\frac{1}{6} f_s$, which leads to a non-minimum phase behavior of the grid-side current [12]. Hence, the proportional feedback gain of the capacitor current should be properly designed. Furthermore, the identification of the range of the gain K_{ad} which guarantees the stability of the system is essential for designing a well-tuned controller.

B. Range of Feedback Gain for Stability of the System

After the capacitor current feedback to the control loop, the equivalent control plant G'_{i_2} can be expressed by (15):

$$\begin{aligned} G'_{i_2}(s) &= \frac{1}{L_1 L_2 C s^3 + G_{td}(s) K_{ad} L_2 C s^2 + L_2) s} \\ &= \frac{1}{L_1 L_2 C s} \frac{1}{s^2 + K_{ad} G_{td}(s)/L_1 s + \omega_r^2} \end{aligned} \tag{15}$$

Based on the previously discussed control elements of the controlled system, the open-loop transfer function from the reference input to the output grid-side current is derived in (16):

$$\begin{aligned} G_{ol}(s) &= G_c(s) G_d G'_{i_2}(s) \\ &= \frac{G_c(s) G_{td}(s)}{L_1 L_2 C s (s^2 + K_{ad} G_{td}(s)/L_1 s + \omega_r^2)} \end{aligned} \tag{16}$$

In order to derive the analytical formulations from the delay-influenced system, the delay $G_d(s)$ can be approximated with the rational polynomial form in (17):

$$G_{td}(s) = e^{-\text{sT}_d} = (\frac{1 - \frac{T_d s}{2n}}{1 + \frac{T_d s}{2n}})^n \tag{17}$$

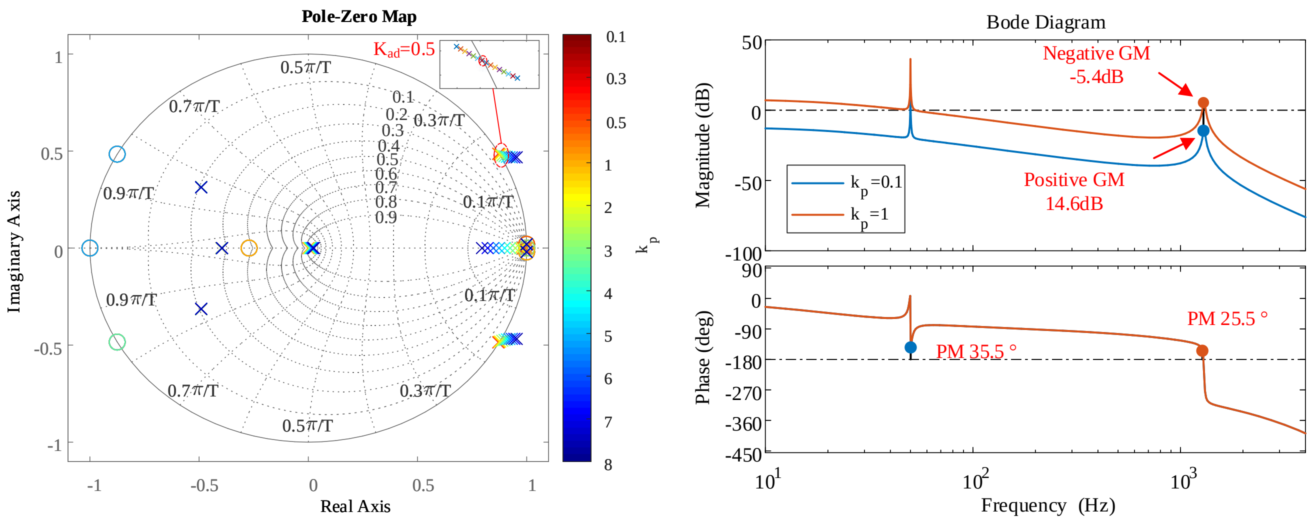

(a) (b)

Fig. 4. Control loop without active damping (a) Poles-zeros map (b) Bode Plot.

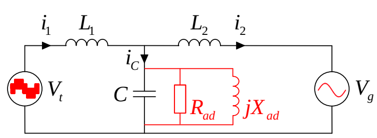

Fig. 5. Equivalent circuit of the LCL-filter based integration of the grid-connected VSC.

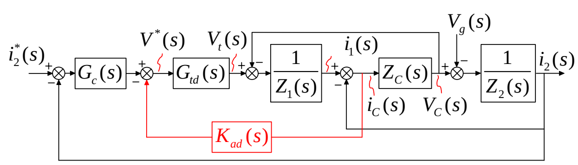

Fig. 6. Block diagram using CCAD control.

where n= 2 can give a precise approximation. Therefore, it can be noted that the pole of the open-loop can be located in the right-half part of the s plane or outside the unit circle of the corresponding z plane, with the increase of the feedback gain. Thus, the critical $K_{\text{ad\_c}}$ is defined as the gain which proceeds a imaginary pole $s = j\omega_{\text{x}}$, namely

$$pole(G_{\text{ol}}(j\omega_{\text{x}})) = 0 \tag{18}$$

Substitute (16) and (17) into (18), ω_{x} is solved as:

$$\begin{aligned} \omega_{\text{x}} &= \sqrt{\frac{-b - \sqrt{b^2 - 4ac}}{2a}} \\ a = (\frac{T_{\text{d}}}{4})^4, &\quad b = -\frac{3}{8}T_{\text{d}}^2, \quad c = 1, \end{aligned} \tag{19}$$

and $K_{\text{ad\_c}}$ hence is expressed in (20):

$$K_{\text{ad\_}c} = \frac{(\omega_{\text{x}}^2 - \omega_{\text{r}}^2)(1 + \omega_{\text{x}}^2 T_{\text{d}}^2/16)^2 L_1}{\omega_{\text{x}}^2 T_{\text{d}}^2 (1 - \omega_{\text{x}}^2 T_{\text{d}}^2/16)} \tag{20}$$

From (19) and (20), it is observed that the imaginary pole ω_{x} is the new resonance frequency shifted by the delay and it is solely determined by the value of the delay. Meanwhile, the maximum feedback gain K_{ad} allowing non-right-half-plane (RHP) poles is restrained by the LCL filter parameters and delay together. Above $K_{\text{ad\_c}}$, the system can be still stable despite the open-loop poles located in RHP. Since the open-loop system has one pair of conjugate poles in the RHP, the boundary of this gain can be derived by forcing the open-loop system encircle the point (-1,0) once anti-clock-wisely in the half nyquist plot, where ω increases from 0 to ∞. Since the $-180°$ crossing occurs at ω_{x}, it can be mathematically expressed as:

$$|G_{\text{ol}}(j\omega_{\text{x}})| \geq 1 \tag{21}$$

The upper boundary $K_{\text{ad\_u}}$ is then derived in (22).

$$\begin{aligned} K_{\text{ad\_u}} &= \frac{(\Delta\omega^2 + \omega_{\text{x}}^2 - \omega_{\text{r}}^2)(1 + \omega_{\text{x}}^2 T_{\text{d}}^2/16)^2 L_1}{\omega_{\text{x}}^2 T_{\text{d}}^2 (1 - \omega_{\text{x}}^2 T_{\text{d}}^2/16)} \\ \Delta\omega^2 &= \frac{\sqrt{k_{\text{p}}^2 + (k_{\text{r}}/\omega_{\text{x}})^2}}{\omega_{\text{x}} L_1 L_2 C} \approx \frac{k_{\text{p}}}{\omega_{\text{x}} L_1 L_2 C} \end{aligned} \tag{22}$$

The expression (22) shows that the maximum feedback gain for achieving stability of the close-loop system is altogether determined by the controller parameters, the time delay and the LCL filter parameters. The difference between this gain and the previously derived $K_{\text{ad\_c}}$ points out that the controlled VSC with LCL filter can be still stable with the control of the current controller despite the open-loop poles in the RHP. However, such an unstable open-loop system is not preferred in practice and thus $K_{\text{ad\_c}}$ is taken as the maximum set value:

$$K_{\text{ad-max}} = K_{\text{ad\_c}} \tag{23}$$

The minimum value of K_{ad} can be obtained by forcing the open-loop system to not encircle the point (-1,0) in the nyquist

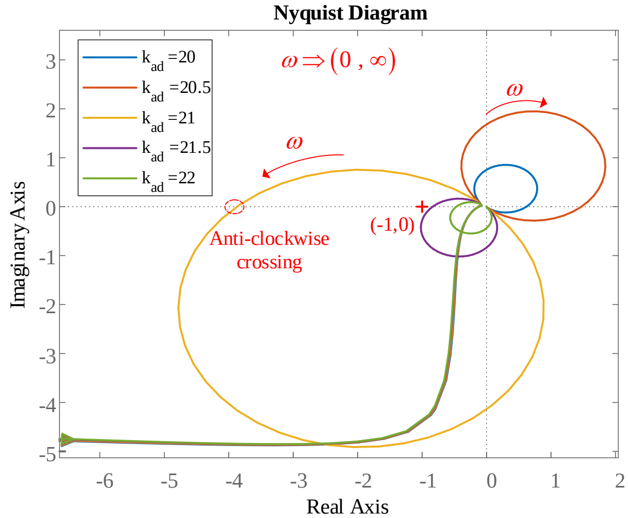

Fig. 7. Nyquist plot of the open-loop system (half-plot).

plot. The $-180°$ occurs at the resonance frequency ω_r, hence it can be mathematically expressed in (24):

$$|G_{ol}(j\omega_r)| \leq 1 \tag{24}$$

which yields (25).

$$K_{\text{ad-min}} = \frac{\sqrt{k_p^2 + (k_r/\omega_r)^2}}{\omega_r^2 L_2 C} \approx \frac{k_p}{\omega_r^2 L_2 C} \tag{25}$$

Specifically, $K_{\text{ad-min}}$ is equal to $k_p/2$ when $L_1 = L_2$ is satisfied. Therefore, the suitable range of feedback gain is:

$$K_{ad} \in (K_{\text{ad-min}}, K_{\text{ad-max}}) \tag{26}$$

Based on the parameters in Table.I, the pzmap of the close-loop system and the bode plot of the open-loop system are drawn in Fig.8, when the controller gain k_p is chosen as 5. $K_{\text{ad\_c}}$ and $K_{\text{ad\_u}}$, as well as $K_{\text{ad}-\min}$, are indicated in Fig.8a, which coincide with the calculated values based on the derived equations. Besides, Fig.8b shows the bode plot of the open-loop system with different K_{ad}, which presents the shifted resonance and the negative $-180°$ crossing. Fig.7 demonstrates the nyquist plot of the open-loop system with the K_{ad} around $K_{\text{ad\_c}}$ and $K_{\text{ad\_u}}$. As the gain exceeds $K_{\text{ad\_c}}$, a negative $-180°$ along with a resonance (>1 dB) occurs in the bode plot which corresponds the one anti-clockwise encirclement of (-1,0) in the half nyquist plot. Meanwhile, the open-loop system has one conjugate pair of RHP poles. According to the nyquist stability criterion, the close-loop system is stable as the numbers of anti-clockwise encirclement equal the number of open-loop RHP poles. However, after k_{ad} becomes larger than $K_{\text{ad\_u}}$, the resonance is smaller than 1 dB which means there is no encirclement of (-1,0). Hence, the close-loop system has the same numbers of RHP poles as the open-loop system has.

C. Stability Margins

In order to achieve stable control, an appropriate gain and phase margin should be guaranteed by properly setting up the feedback gain K_{ad} and controller gain k_p. The gain and phase margins of the controlled system are given by (27):

$$\begin{aligned} GM &= -20\,\text{lg}|G_{ol}(j\omega_r)| \\ PM &= \pi + \angle|G_{ol}(j\omega_{co})| \end{aligned} \tag{27}$$

where ω_{co} is the gain crossover frequency where the open-loop gain $|G_{ol}(j\omega)|$ reaches 1 and the phase crossover frequency is equal to ω_r. The gain margin can be further expressed in (28):

$$\begin{aligned} GM &= -20\,\text{lg}\left|\frac{\sqrt{k_p^2 + (k_r/\omega_r)^2}}{K_{ad}\omega_r^2 L_2 C}\right| \\ &\approx -20\,\text{lg}\left|\frac{k_p}{K_{ad}\omega_r^2 L_2 C}\right| \\ &\approx 20(\text{lg}(\frac{K_{ad}}{k_p}) + \text{lg}(\omega_r^2 L_2 C)) \end{aligned} \tag{28}$$

It can be noted that for a given LCL filter, the phase margin is proportional to K_{ad} and inversely proportional to k_p in logarithmic scale. To express the phase margin analytically, the gain crossover frequency is approximated in (29):

$$\begin{aligned} &\omega_{co} \approx \sqrt{\frac{-b + \sqrt{b^2 - 4ac}}{2a}} \\ &a = (\frac{K_{ad}}{L_1})^2, \quad b = \omega_r^4, \quad c = -(\frac{k_p}{L_1 L_2 C})^2 \end{aligned} \tag{29}$$

The phase margin can be further derived in (30):

$$\begin{aligned} PM =& \frac{\pi}{2} - \omega_{co}T_d - tan^{-1}(\frac{k_r}{\omega_{co}k_p}) \\ &- tan^{-1}(\frac{\omega_{co}K_{ad}cos(\omega_{co}T_d)}{L_1(\omega_r^2 - \omega_{co}^2 - \omega_{co}sin(\omega_{co}T_d))}) \end{aligned} \tag{30}$$

The derived relations are plot in Fig.9. It is noteworthy that both the gain and phase margin drop with the increase of K_{ad}. Usually, a gain margin with 10 dB guarantees a good stability. The corresponding K_{ad} is derived as 8, which indicates a phase margin of 69°.

IV. Harmonics Compensation based on Resonant Controller

Harmonics resonators are widely used for suppressing the harmonics caused by the grid distortions by simply introducing single or multiples resonators tuned at the corresponding harmonics frequencies in parallel with the basic current controller. The generalized non-ideal resonators with two integrators [19] in $\alpha\beta$ frame are expressed in (31):

$$G_h(s) = \sum_{h=3,5,7\ldots} K_{ph} + \frac{2K_{rh}\omega_c s}{s^2 + 2\omega_c s + (h\omega_1)^2} \tag{31}$$

where K_{rh} and ω_c represent the resonant controller gain and cut-off frequency (or damping factor) respectively. The bandwidth is adjusted by setting ω_c appropriately. A small

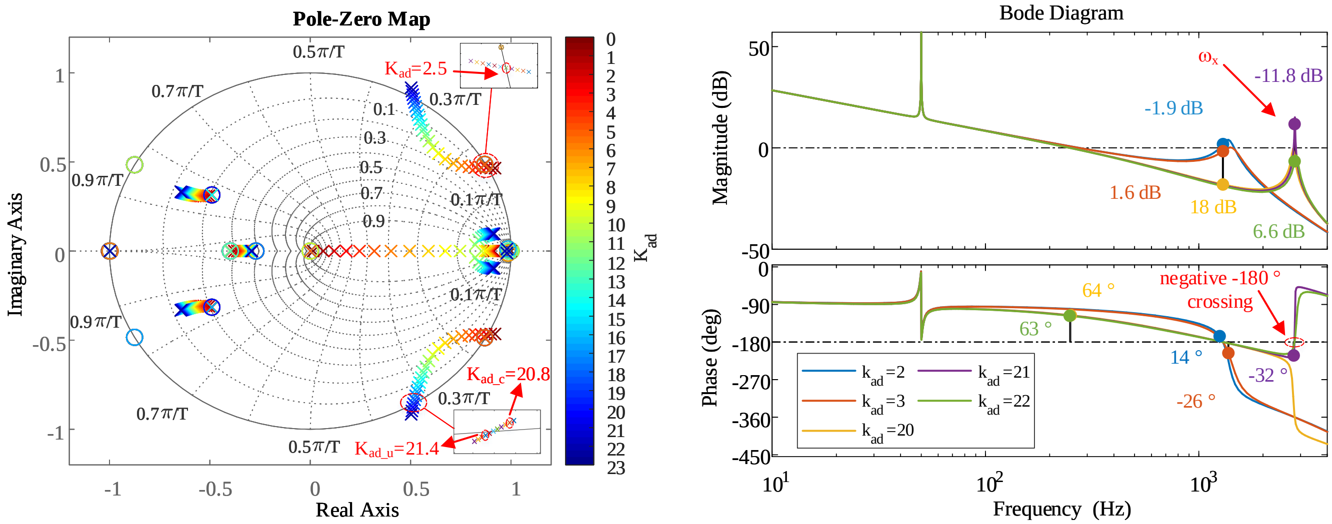

(a) (b)

Fig. 8. Control loop with Capacitor-current feedback ($k_p = 5$) (a) Poles-zeros map (b) Bode Plot.

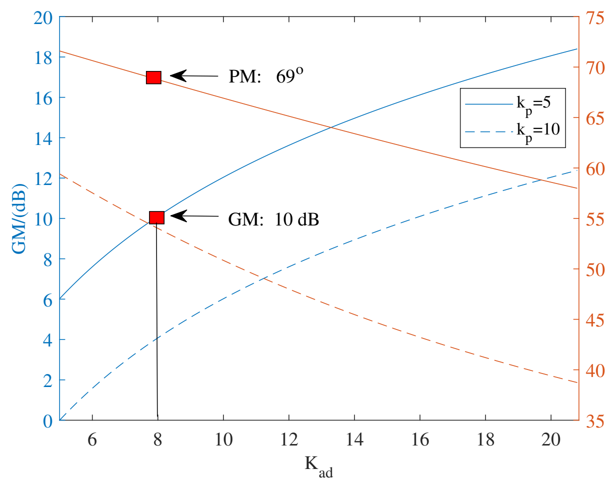

Fig. 9. Gain and Phase Margin versus K_{ad}.

cut-off frequency is usually chosen for high rejection performance [19]. One typical problem associated with the resonators is the phase deterioration caused by the delay. This can be improved by certain phase compensation methods, for example the introduction of a lead-filter [2] cascaded with the resonant controller. The generalized form of a lead filter (F_{lead}) is given by (32)

$$F_{lead} = \frac{s/\omega_f + 1}{s\alpha/\omega_f + 1} \tag{32}$$

where ω_f and α are the tuning parameters determined by the required phase compensation ϕ_{max} at the specified frequency ω_{max}, which is described in (33).

$$\begin{aligned} \sqrt{\alpha} &= tan(\frac{\pi}{4} - \frac{\phi_{max}}{4}) \\ \omega_f &= \omega_{max}\sqrt{\alpha} \end{aligned} \tag{33}$$

The bode plot in Fig.10 shows that the phase at the resonance frequency is improved by the lead filters and the phase margin is hence increased.

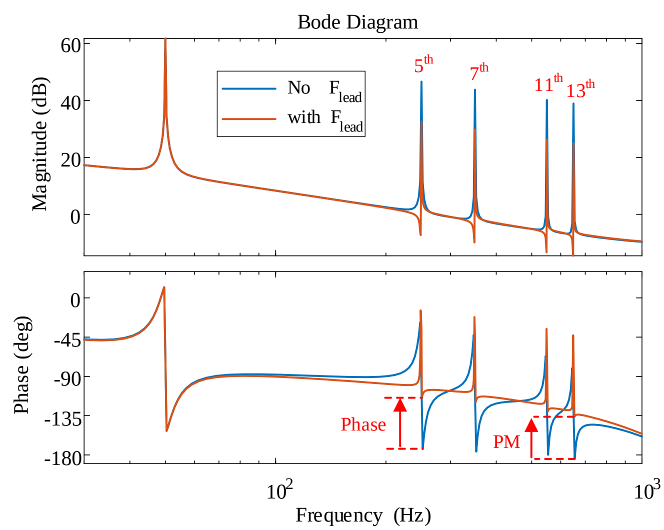

Fig. 10. Bode plot of the open-loop with harmonics resonators.

V. Simulation and Experimental Verification

A. Simulation Results

To verify the accuracy of the identified range of the capacitor-current feedback gain, simulations are conducted in MATLAB/SIMULINK. The operating parameters are listed in Table I. The system operates in inverter mode at a power $P_{ac} = 3\,\text{kW}$ with a feedback current control loop connected to a 400 V 50 Hz 3-phase grid.

Fig.11 shows the grid-side current waveform with different K_{ad} values under an ideal sinusoidal voltage. At $K_{ad} = 2.6$,

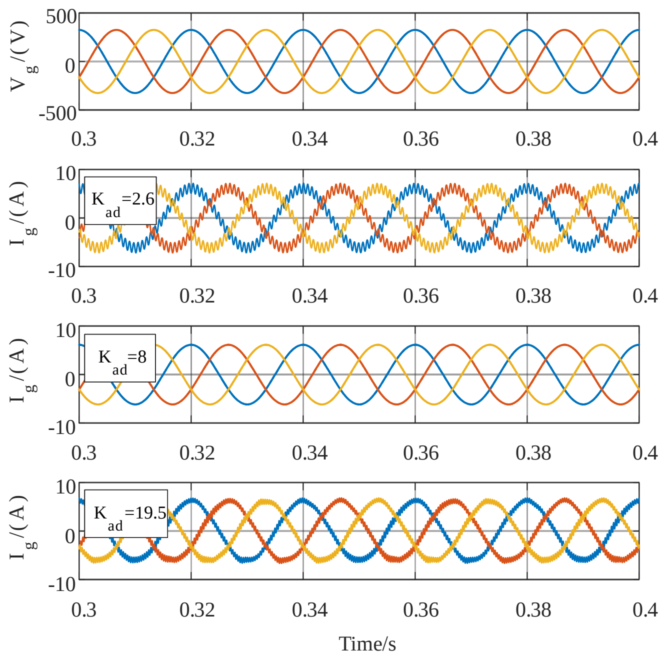

Fig. 11. Simulation results: grid voltages and grid-side currents under different K_{ad}.

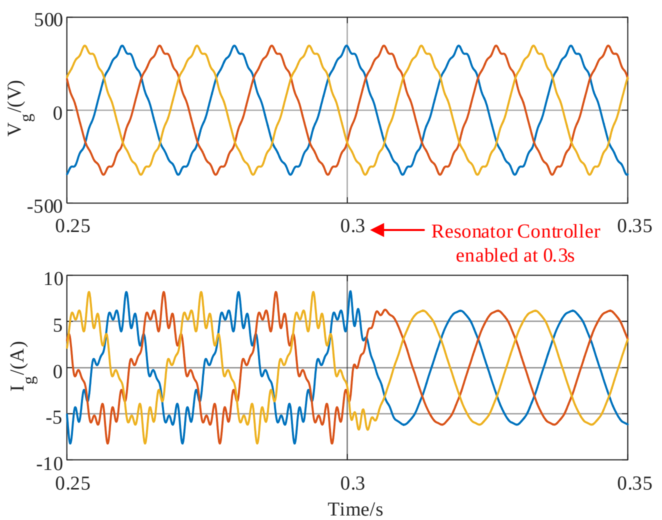

Fig. 12. Simulation results: grid voltages and grid-side currents with the proposed harmonics control.

which is close to the theoretical value 2.5, the grid -side current becomes marginally stable and the resonance occurs in the waveform with the frequency of ω_{r} (1300 Hz). With $K_{\mathrm{ad}} = 8$, at which the system is supposed to have a GM of 10 dB and PM of 69°, the grid-side current follows close to a sinusoidal 50 Hz waveform. After the K_{ad} increases to 19.5, the new resonance component arises in the grid-side current, the frequency of which is around the shifted resonance frequency ω_{x} (2800 Hz). Therefore, the stability range identified from the simulation is close to the theoretical one [2.5,20.8].

The simulation of the harmonics control is shown in Fig.12, where the distorted grid voltage containing low-order frequency harmonics with amplitudes of 5% of the fundamental rated voltage at the 5^{th}, 7^{th}, 11^{th}, 13^{th} is considered. The proposed resonator parameters are listed in Table.I and the lead filters are designed to provide 60° at each harmonics frequency. The harmonics control is enabled at 0.3 s and the results show that the harmonics components in the grid-side current is quickly rejected by the resonators and the current achieves a satisfactory THD of about 0.5%.

B. Experimental Verification

The experimental part of this paper is conducted in a commercial two-level VSC, i.e. Triphase/PM5F30C. The system is set to operate as a shunt active filter generating 1000 VAR reactive power to the distorted grid. The grid voltage is depicted in Fig.13, which contains in relation to the fundamental frequency component: 0.5% 5^{th}, 2%7^{th}, 0.5% 11^{th}, 0.3%13^{th}. As expected, the grid-side current is severely distorted due to the considerable filter capacitor, which leads to a quite large low-order harmonics in the current. Hence, the results in Fig.13 show the same tendency as the simulation results in Fig.12. Note that the system is still stable even without the capacitor-current feedback ($K_{\mathrm{ad}} = 0$). This is due to the quite large internal resistance of the LCL filter and inherent damping caused by the inefficient semiconductors in the Triphase system (high switching and conduction losses). The resonance (at $\omega_{\mathrm{r}} = 1300$ Hz) in the grid-side current at $K_{\mathrm{ad}} = 0$ shows that the system is close to the marginally stable condition. At $K_{\mathrm{ad}} = 7$, only low-order harmonics exist in the grid-side current. After K_{ad} reaches 13, the system becomes marginally stable and the resonance (at $\omega_{\mathrm{x}} = 2800$ Hz) quickly arises. The maximum K_{ad} is smaller than the theoretical one and this can be explained by the fact that the delay and the damping characteristics in the system are different from the simulated system. In the final paper the parameters will be tuned accordingly so both simulation and experimental results are better matched. Fig.14 presents the grid-side current with and without the harmonics control under $K_{\mathrm{ad}} = 7$. After the implementation of the proposed resonator, the THD of the grid-side current decreased from 32% to 7.5%, which is still quite large. This might be because that the insufficient phase compensation limits the further increase of k_{rh} and ω_{c}.

VI. Conclusion and Future Work

This paper derives the boundaries of the capacitor-current feedback gain to realize effective active damping. Besides, a harmonics resonator cascaded with lead filter is proposed to compensate the selective harmonics components in the grid-side current due to the distorted grid voltage. Both simulation and experimental results show the performance of the proposed control scheme. However, the practical results deviates from the theoretical and simulation results due to the unidentified damping and delay in the practical system. The effectiveness of the resonator is so far limited by the current achieved phase

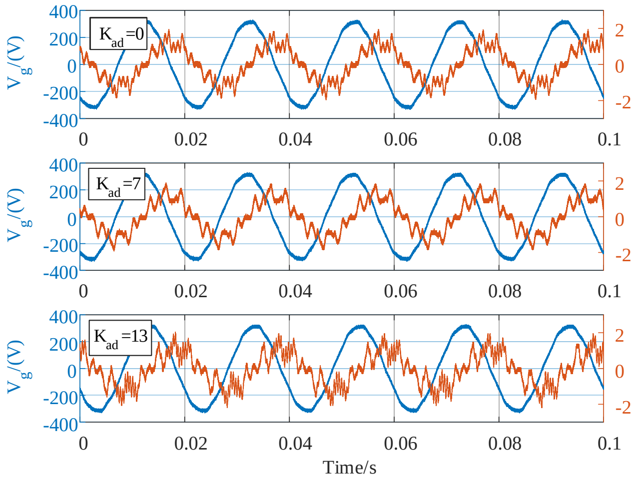

Fig. 13. Preliminary experimental results: Grid-side current under different K_{ad}.

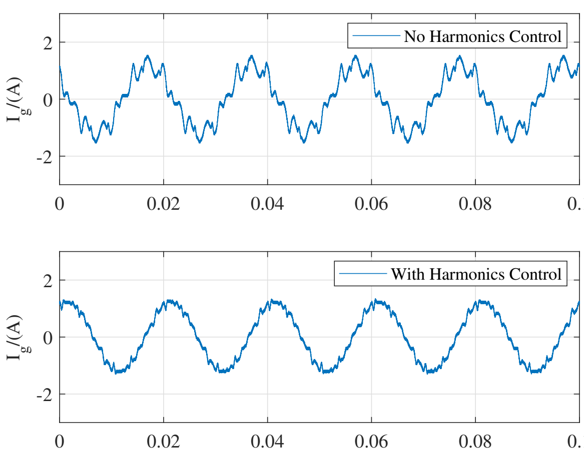

Fig. 14. Preliminary experimental results: Grid-side current with harmonics control under distorted grid voltage.

margin. However, in the final paper additional improved experimental results will be included addressing those differences. Therefore, future work will focus on more effective phase compensation methods and other harmonics control techniques i.e, multiple-axis control and full grid voltage feed-forward strategy.

References

[1] F. Blaabjerg, R. Teodorescu, M. Liserre, and A. V. Timbus, "Overview of control and grid synchronization for distributed power generation systems," *IEEE Transactions on Industrial Electronics*, vol. 53, no. 5, pp. 1398–1409, Oct 2006.

[2] Y. Wu, A. Shekhar, T. B. Soeiro, and P. Bauer, "Voltage source converter control under distorted grid voltage for hybrid ac-dc distribution links," in *IECON 2019 - 45th Annual Conference of the IEEE Industrial Electronics Society*, vol. 1, 2019, pp. 5694–5699.

[3] A. Shekhar, T. B. Soeiro, Y. Wu, and P. Bauer, "Optimal power flow control in parallel operating ac and dc distribution links," *IEEE Transactions on Industrial Electronics*, vol. 68, no. 2, pp. 1695–1706, 2020.

[4] A. Shekhar, L. B. Larumbe, T. B. Soeiro, Y. Wu, and P. Bauer, "Number of levels, arm inductance and modulation trade-offs for high power medium voltage grid-connected modular multilevel converters," *ICPE-ECCE Asia IEEE*, 2019.

[5] J. Xu, J. Han, Y. Wang, S. Habib, and H. Tang, "A novel scalar pwm method to reduce leakage current in three-phase two-level transformerless grid-connected vsis," *IEEE Transactions on Industrial Electronics*, vol. 67, no. 5, pp. 3788–3797, 2020.

[6] J. Xu, J. Han, Y. Wang, M. Ali, and H. Tang, "High-frequency sic three-phase vsis with common-mode voltage reduction and improved performance using novel tri-state pwm method," *IEEE Transactions on Power Electronics*, vol. 34, no. 2, pp. 1809–1822, 2019.

[7] J. Wang, J. D. Yan, L. Jiang, and J. Zou, "Delay-dependent stability of single-loop controlled grid-connected inverters with lcl filters," *IEEE Transactions on Power Electronics*, vol. 31, no. 1, pp. 743–757, Jan 2016.

[8] S. G. Parker, B. P. McGrath, and D. G. Holmes, "Regions of active damping control for lcl filters," in *2012 IEEE Energy Conversion Congress and Exposition (ECCE)*, Sep. 2012, pp. 53–60.

[9] C. Zou, B. Liu, S. Duan, and R. Li, "Influence of delay on system stability and delay optimization of grid-connected inverters with lcl filter," *IEEE Transactions on Industrial Informatics*, vol. 10, no. 3, pp. 1775–1784, Aug 2014.

[10] R. Peña-Alzola, M. Liserre, F. Blaabjerg, R. Sebastián, J. Dannehl, and F. W. Fuchs, "Analysis of the passive damping losses in lcl-filter-based grid converters," *IEEE Transactions on Power Electronics*, vol. 28, no. 6, pp. 2642–2646, June 2013.

[11] J. Dannehl, M. Liserre, and F. W. Fuchs, "Filter-based active damping of voltage source converters with *lcl* filter," *IEEE Transactions on Industrial Electronics*, vol. 58, no. 8, pp. 3623–3633, Aug 2011.

[12] X. Wang, F. Blaabjerg, and P. C. Loh, "Virtual rc damping of lcl-filtered voltage source converters with extended selective harmonic compensation," *IEEE Transactions on Power Electronics*, vol. 30, 10 2014.

[13] W. Yao, Y. Yang, X. Zhang, F. Blaabjerg, and P. C. Loh, "Design and analysis of robust active damping for lcl filters using digital notch filters," *IEEE Transactions on Power Electronics*, vol. 32, no. 3, pp. 2360–2375, March 2017.

[14] S. Leitner, M. Yazdanian, S. Ziaeinejad, A. Mehrizi-Sani, and A. Muetze, "Internal model-based active resonance damping current control of a grid-connected voltage-sourced converter with an lcl filter," *IEEE Transactions on Power Systems*, vol. 33, no. 6, pp. 6025–6036, Nov 2018.

[15] R. Peña-Alzola, M. Liserre, F. Blaabjerg, M. Ordonez, and T. Kerekes, "A self-commissioning notch filter for active damping in a three-phase lcl -filter-based grid-tie converter," *IEEE Transactions on Power Electronics*, vol. 29, no. 12, pp. 6754–6761, Dec 2014.

[16] R. Peña-Alzola, M. Liserre, F. Blaabjerg, R. Sebastián, J. Dannehl, and F. W. Fuchs, "Systematic design of the lead-lag network method for active damping in lcl-filter based three phase converters," *IEEE Transactions on Industrial Informatics*, vol. 10, no. 1, pp. 43–52, Feb 2014.

[17] D. Pan, X. Ruan, C. Bao, W. Li, and X. Wang, "Capacitor-current-feedback active damping with reduced computation delay for improving robustness of lcl-type grid-connected inverter," *IEEE Transactions on Power Electronics*, vol. 29, no. 7, pp. 3414–3427, July 2014.

[18] X. Wang, X. Ruan, S. Liu, and C. K. Tse, "Full feedforward of grid voltage for grid-connected inverter with lcl filter to suppress current distortion due to grid voltage harmonics," *IEEE Transactions on Power Electronics*, vol. 25, no. 12, pp. 3119–3127, Dec 2010.

[19] R. Teodorescu, F. Blaabjerg, M. Liserre, and P. Loh, "Proportional-resonant controllers and filters for grid-connected voltage-source converters," *Electric Power Applications, IEE Proceedings -*, vol. 153, pp. 750 – 762, 10 2006.

[20] A. G. Yepes, F. D. Freijedo, Lopez, and J. Doval-Gandoy, "High-performance digital resonant controllers implemented with two integrators," *IEEE Transactions on Power Electronics*, vol. 26, no. 2, pp. 563–576, Feb 2011.

[21] A. G. Yepes, F. D. Freijedo, J. Doval-Gandoy, López, J. Malvar, and P. Fernandez-Comesaña, "Effects of discretization methods on the performance of resonant controllers," *IEEE Transactions on Power Electronics*, vol. 25, no. 7, pp. 1692–1712, July 2010.